Composition Dependence of Lithium Diffusion in Lithium Silicide: a Density Functional Theory Study

Zhiguo Wang,[1*] Qiulei Su,[2] Huiqiu Deng,[2] Y.Q. Fu[3*]

1 *School of Physical Electronics, University of Electronic Science and Technology of China, Chengdu, 610054, P.R. China*
2 *Department of Applied Physics, Hunan University, Changsha 410082, P.R. China*
3 *Department of Physics and Electrical Engineering, Faculty of Engineering and Environment, University of Northumbria, Newcastle upon Tyne, NE1 8ST, UK*

[*]Corresponding author. E-mail: zgwang@uestc.edu.cn (ZW); richard.fu@northumbria.ac.uk (YF)

ABSTRACT: In this work, lithiation process of silicon was investigated using *ab initio* molecular dynamics. Diffusion coefficients of Li in Li-Si alloys were calculated to be in the range between 2.08×10^{-9} $cm^2\cdot s^{-1}$ and 3.53×10^{-7} $cm^2\cdot s^{-1}$ at room temperature. Results showed that the Li mobility is strongly dependent on the composition of the Li_xSi alloys. The Li diffusivity in the Li_xSi alloy can be enhanced by two orders of magnitude when x is increased from 1.0 to 3.75, which can be explained by the instability of the Si network due to the charge transfer from Li to Si.

KEYWORDS: Silicon lithiation; Composition dependence; Density functional theory

1. Introduction

Due to the huge demands for energy storage and continued miniaturization of portable devices/consumer electronics, there is a stringent requirement for longer lasting portable energy storage systems with high power densities.[1] Binary lithium alloys (such as Li_xSi, Li_xGe and Li_xSn) have been considered as the suitable anode materials because of their larger specific capacities compared to graphite, which is currently widely used in lithium ion batteries. The gravimetric energy density of silicon is 3579 $mAh \cdot g^{-1}$,[2] which is about 10 times as large as that of graphite (372 $mAh \cdot g^{-1}$).[3] Unfortunately, Si suffers from large volume changes upon alloying with Li, which frequently cause Si anode to crack and pulverize, thus leading to its premature failure and poor cycle life time.[4] Considerable effort has been made to improve the capacity of Si anodes by structural modifications such as using nano-structured Si based materials (i.e., Si nanowires and SiC nanocomposites)[5], and alloying with active/inactive elements.[6] Lithiation of crystalline Si results in different structural changes compared with those from transition metal oxides or graphitic electrode materials, where Li is intercalated into the Si lattice sites with structural distortions. Crystalline Si is generally changed into amorphous lithium silicide upon lithiation, and the phase transitions in the Li_xSi alloys during Li insertion have been investigated using various techniques, such as scanning electron microscopy[7], *in-situ* X-ray diffraction (XRD)[8], *ex-situ* XRD[9], *in-situ* transmission electron microscopy analysis[10] and real time nuclear magnetic resonance (NMR)[11].

Large values of Li diffusivity in electrode materials are preferred for the development of rechargeable batteries with an optimum performance. The diffusivity value of Li in a vacuum-deposited silicon film on a Ni substrate was measured to be 10^{-9} $cm^2 \cdot s^{-1}$ at 298 K,[12] whereas the value obtained from a single crystalline silicon plate was 2×10^{-11} $cm^2 \cdot s^{-1}$.[12] The relatively larger

value obtained with the vacuum-deposited Si film was attributed to the relatively porous/columnar structures of the Si film.[12] There were two types of Li diffusion processes in the crystalline $Li_{12}Si_7$ alloy with activation energies of 0.32 and 0.55 eV obtained from NMR measurements.[13] Due to complexity of the experimental measurements, and difficulty in controlling the precise conditions/parameters, it is quite complicated to experimentally obtain the true values of diffusivity of Li. From literature, there is a large discrepancy existed for the experimentally obtained values of diffusivity of Li in Si, spanning four orders of magnitudes, between 10^{-14} and 10^{-10} $cm^2 \cdot s^{-1}$, with an average value of 10^{-12} $cm^2 \cdot s^{-1}$.[12, 14]

Density functional theory (DFT)-based methods can provide an atomic-level description of diffusion mechanisms in solids, which is a prerequisite for a better understanding of the lithiation process and its diffusion kinetics. *Ab initio* calculations were frequently used to investigate the lithiation of both crystalline and amorphous Si.[15] To study the lithiation behavior at the onset stage, most work was focused on insertion of single Li atom into Si with different axis orientations and sizes.[15a-g] However, with increasing the Li content in the Si, Li_xSi alloys will form, thus it is critical to theoretically determine the diffusivity of Li in the Li_xSi alloys with various Li contents. *Ab initio* molecular dynamics were frequently used to study the crystalline to amorphous phase transition of the Li-Si alloys.[16] For example, Johari et al. [16a] investigated the diffusivity of Li in Si using the *ab initio* molecular dynamics. The diffusivity of Li in crystalline Si anode at 298 K was found to be 4.88×10^{-9} $cm^2 \cdot s^{-1}$, with an energy barrier of 0.33 eV for Li diffusion into Si. Jung et al.[17] reported that the diffusivity of Li in $Li_{3.7}Si$ alloys at a temperature of 300 K was 1.8×10^{-8} $cm^2 \cdot s^{-1}$. Chou and Hwang[18] reported that the diffusivity of Li in amorphous $Li_{3.57}Si$ at a temperature of 298 K was 1.66×10^{-7} $cm^2 \cdot s^{-1}$. Due to the large discrepancy and scattering of the experimental values, it is important to systemically and

theoretically study the composition dependent diffusion in the Li-Si alloys in order to clarify the true mechanisms for different lithiation stages in Si.

In this work, we used DFT-based *ab initio* molecular dynamics to determine the diffusivity of Li in Li_xSi alloys with various Li contents (x=1.00, 1.71, 3.25 and 3.75), in order to understand the lithiation mechanisms of the Si based anode materials, and provide fundamental data on the diffusion of Li in Si.

2. Results and Discussion

The electronic and structural properties of the crystalline LiSi, $Li_{12}Si_7$, $Li_{13}Si_4$, $Li_{15}Si_4$, which can be represent with Li_xSi (x=1.00, 1.71, 3.25 and 3.75) were studied by using a double-ζ basis set (DZ) and double-ζ basis set plus polarization functions (DZP). The calculated lattice constants are summarized in Table 1. The structural data in Table 1 agree well with experimental studies and previous theoretical work.[19] As the electronegativity of the Si atom is not large enough to completely accept all the electrons from the Li atoms, thus most of the Li-Si alloys do not follow an electron counting rule ((8-*N*) rules)[20]. Therefore, the Li atoms do not donate all their valence electrons to Si atoms, so the Li_xSi shows different connectivity depending on the x value. The pair-correlation function (PCF) calculated for Si-Si, Li-Li, and Li-Si pairs in crystalline LiSi, $Li_{12}Si_7$, $Li_{13}Si_4$, $Li_{15}Si_4$ are shown in Fig. 1, together with their atomic structures. The PCF is defined as the number of neighboring atoms of a given atom per unit volume as a function of distance, and provides important structural and bonding information for both the crystalline and amorphous solids. Green and red balls represent the Si and Li atoms, respectively. The coordination number (CN) calculated for the first nearest neighbor is presented in Table 2. Fig. 1 and Table 2 show the connectivity in the crystalline Li_xSi alloys. In a LiSi alloy, each Si

atom has three Si neighbors with a Si-Si bond length of 2.45 Å. In the $Li_{12}Si_7$ alloy, there are planar 5Si-rings with a Si-Si bond length of 2.39 Å and a planar Si 'Y'-shape with a bond length of 2.42-2.45 Å. In the $Li_{13}Si_4$ alloy, half of the Si atoms are in the forms of Si dumbbells with a Li-Si bond length of 2.49 Å, while the other half atoms are surrounded by the Li atoms with a Li-Si bond length of 2.47 Å. The Si frameworks show a decrease in connectivity with increasing x value, and the $Li_{15}Si_4$ phase has only isolated Si atoms: i.e., there is no Si-Si bond within the length of 4.48 Å. The data of density of states (DOS) projected on the Si and Li atoms in crystalline LiSi, $Li_{12}Si_7$, $Li_{13}Si_4$, $Li_{15}Si_4$ are shown in Fig. 2. The Fermi energy level is set to be zero. The results of the DOS also confirm the decrease of Si-Si connectivity with increasing Li content. As the Li fraction is changed from 1 (LiSi) to 3.75 ($Li_{15}Si_4$) per Si in crystalline Li-Si alloys, the splitting between the Si 3*s* and Si 3*p* states becomes larger and the distribution of the Si 3*s* and Si 3*p* states becomes narrower, which is attributed to the decreasing Si-Si bond interactions.[21] The DOS calculated with the double-ζ basis set plus polarization functions is the same with that calculated with double-ζ basis set, which indicates that double-ζ basis set is enough to be used in the calculations for this study.

Experimental results confirmed that the crystalline Si is changed into amorphous lithium silicide upon electrochemical insertion of Li atoms during initial lithiation process. The atomistic details of the amorphization process were investigated using *ab initio* molecular dynamics. There is no apparent difference of atomic evolution upon lithiation of Si into Li_xSi alloys (x=1.00, 1.71, 3.25 and 3.75). Fig. 3 shows structural snapshots of lithiation process of Si and formation of amorphous $Li_{3.25}Si$ alloy at 1300 K. The Li atoms are inserted gradually into the Si lattice by breaking and expanding the Si-Si bonds. Upon alloying with Li, the tetrahedrally bonded Si network is weakened and changed into low-connectivity clusters due to the excess charges

transferred from the Li.[16b, 22] The Si atoms are relatively stationary at the initial lithiation step. The Si lattice structure shows no apparent expansion at a simulation time of 0.4 ps, although the Li atoms penetrate into the Si lattice. The Si diffuses into Li at a time of 0.8 ps. The diffusion rate of Si is less than that of Li as shown in Fig. 3 at a simulation time of 8.7 ps. At a simulation time of 15 ps, the Li and Si atoms are fully mixed, which indicates that 15 ps is sufficient enough for a substantial lithiation process of Si.

In order to provide further evidence of the lithiation induced crystal-to-amorphous transition, the PCF was calculated for the Si-Si, Li-Li, and Li-Si pairs upon lithiation. The values of PCF calculated for the Si-Si, Li-Li, and Li-Si pairs upon lithiation of Si to form amorphous $Li_{3.25}Si$ alloy at 1300 K are shown in Fig. 4. From Fig. 4, the PCF peaks of Si-Si and Li-Li decrease, whereas those of Li-Si increase with increasing the lithiation time. This indicates that the numbers of Si-Si and Li-Li neighbors decrease, whereas those of Li-Si neighbors increase upon lithiation. There are several sharp PCF peaks for the Si-Si before lithiation. The first and the second sharp peaks are located at 2.41 and 3.87 Å, respectively, which are corresponding to the first and second nearest Si-Si neighbors in Si. With increasing the simulation time, the sharp peaks at the distances larger than 5 Å disappear. Whereas the peaks at the distances smaller than 5 Å are broadened. This indicates that the long-range order of atomic arrangement disappears and the short-range order still remains. Finally all the sharp peaks disappear, which indicates the formation of amorphization of Si induced by the Li lithiation. After the full lithiation, the nearest neighboring distance becomes 2.71 Å for Li-Si and 2.63 Å for Li-Li. There are some Si atoms which remain to be covalently bonded, but their bond distances are slightly increased from 2.41 to 2.65 Å after the full lithiation. This is caused by the softening of the Si-Si bond after the electrons are transferred from Li to Si.

Fig. 5 shows the calculated average values of the MSDs for the Li and Si atoms as a function of simulation time at temperatures from 1100 to 1500 K. As expected, the values of the MSDs increase with the simulation time. However, the slope increases with the temperature, indicating a faster lithiation process at a higher temperature. The increase of the MSDs for the Si is slower than that for the Li. The values of diffusivity at room temperature (i.e., 300 K) are shown in Fig. 6, which was obtained by extrapolating the data of diffusivities of Li and Si at different temperatures. The inset in Fig. 6 shows the value of MSDs for the Li and Si atoms in $Li_{1.71}Si$ at 1300K with k-meshes of 1×1×1 and 2×2×1 and cut-off of 150 and 180 Ry. The curves are overlapped indicating that k-mesh with Γ point and cutoff 150 Ry were enough to be used in the calculations for this study.

The diffusion barrier (E_A) and diffusion coefficients (D) at 300 K obtained using Equation (3) for Li in the Li_xSi alloys (x=1.00, 1.71, 3.25 and 3.75) are shown in Fig. 7. The diffusion barrier and diffusion coefficients of the Li depend on the composition of Li_xSi alloys. The calculated diffusion coefficients are in the range between 2.08×10^{-9} $cm^2\cdot s^{-1}$ to 3.53×10^{-7} $cm^2\cdot s^{-1}$. Experimental data of the diffusivity of Li in Si from literature are in the range between 10^{-14} and 10^{-8} cm^2 s^{-1} [12, 14, 23]. Clearly there are only minor differences between results from this study and those from literature. From Fig. 7, the diffusion coefficients are increased from 2.08×10^{-9} $cm^2\cdot s^{-1}$ to 2.37×10^{-7} $cm^2\cdot s^{-1}$ as the Li contents are increased from x=1.00 to 3.75. This suggests that the diffusion coefficients vary in two orders of magnitude depending on the stages of lithiation. Previous research reported that the diffusion coefficients of lithium varied with the lithium concentration in nano-Si.[14a] Our results show a nearly linear increase of the diffusion coefficients with Li content, which is different from the earlier experimental observation of W-shape changes of diffusion coefficients with Li content.[14a] Experimentally lithiated samples

generally exhibited a certain degree of inhomogeneity in terms of Li concentrations and coexistence of crystalline and amorphous phases. This might cause the differences of the obtained experimental results in literature. The energy barriers decrease with Li contents, which also agrees with the reported values in Ref. [7]. However, the calculated diffusion barriers of Si upon lithiation are 0.55-0.59 eV, which are less dependent on the Li contents. Diffusion coefficients of Si are decreased from 3.02×10^{-12} $cm^2\cdot s^{-1}$ to 8.52×10^{-13} $cm^2\cdot s^{-1}$ as the Li content is increased from x=1.00 to 3.75, as shown in Fig. 7(b). The diffusivity of Si is several orders of magnitude smaller than that of the Li, which suggests that the Si atoms are relatively stable during the lithiation process. We also calculated the diffusion barriers of Li in the crystalline alloys of LiSi, $Li_{12}Si_7$, $Li_{13}Si_4$, $Li_{15}Si_4$ using climbing image nudged elastic band (CI-NEB) theory[24]. The Vienna Ab-initio Simulation Package (VASP) [25] code was used to calculate the composition dependent diffusion. The calculated diffusion barriers through the mechanism of Li vacancy migration are shown in Fig. 7 (a), revealing a path-dependent diffusion, and the diffusion barriers have values of 0.12 and 0.27 eV in $Li_{15}Si_4$. It is interesting to find that the minimum diffusion barriers decrease with increasing Li content, which shows the same trend for Li diffusivity in the Li_xSi alloy upon lithiation.

The increase of the diffusion coefficients with Li content can be explained by the charge transfer from Li to Si. As more Li atoms are lithiated into the Si, more electrons will be transferred to Si, which fills up the anti-bonding sp^3 states of Si. Therefore, the Si network is destabilized by lithiation process, which makes the diffusion of Li much easier. Except for the crystalline Si, amorphous Si can also be used as anode for the LIBs. Generally amorphous Li_xSi alloys are formed upon lithiation of amorphous Si.[10a] The composition dependence of diffusion is also critical to be investigated. We have analyzed the atomistic structure evolution upon

lithation. The atomic configurations after simulation of 0.8 ps are shown in the inset of Fig. 5. It is found that the crystalline Si loses its crystallinity at about 0.8 ps for x=1.00, 1.71, 3.25 and 3.75, so the lithiation process could also be referred as lithiation of amorphous Si after 0.8 ps. Therefore, we could draw the conclusion that the Li diffusivity will be enhanced and Si diffusivity would decrease with increasing of Li content if the amorphous Si is used as anode for the LIBs.

3. Conclusion

The electrochemical lithiation of crystalline Si was studied by using *ab initio* molecular dynamics. The electrochemical process is a non-equilibrium process in which amorphous Li_xSi alloys are formed. The diffusion coefficients can be changed in two orders of magnitude depending on the stages of lithiation. The diffusion coefficients are increased from 2.08×10^{-9} $cm^2\cdot s^{-1}$ to 3.53×10^{-7} $cm^2\cdot s^{-1}$ as the Li content is increased from x=1.00 to 3.75 at room temperature. The diffusivity of Si is several orders of magnitude smaller than that of the Li. These results provide fundamental data on the diffusion of Li in Si, which is important for the design of the alloy electrodes for lithium ion batteries.

4. Simulation Details

A 2×2×2 suppercell (consisting of 64 Si atoms) without coordination defects was used to model the Si anode. The most common crystallographic surfaces for the commercial Si wafers are (100), (110), and (111). Si (100) surface was chosen as the lithiation facet in this work. Volume expansion of the crystalline Si was calculated after it was fully lithiated into amorphous phase Li_xSi (x=1.00, 1.71, 3.25 and 3.75) at 0 K. The volume expansion ratios were about 60%,

110%, 220% and 260% for x=1.00, 1.71, 3.25 and 3.75, respectively. The lithiation process of Li into Si was modeled using the 64 Si-atom supercell with gradually increasing the length along [001]-direction by 60%, 110%, 220% and 260%, respectively. The space above the silicon was initially filled with 64, 110, 208 and 240 Li atoms with an amorphous arrangement.

The lithiation of Si was investigated using *ab initio* molecular dynamics calculations within the framework of DFT using the SIESTA code[26], which adopts a linear combination of numerical localized atomic orbital basis sets for the description of valence electrons and norm-conserving nonlocal pseudo-potentials for the atomic core[27]. The valence electron wave functions were expanded using a double-ζ basis set. The charge density was projected on a real space grid with a cut-off of 150 Ry to calculate the self-consistent Hamiltonian matrix elements, and Γ point was used in the Brillouin zone sampling. The evolution of the system was derived using the molecular dynamics (MD) method with a verlet algorithm and a time-step of 1.0 fs. The LIBs operation was performed at room temperature. We did the simulation for $Li_{1.71}Si$ at 300K with 50000 MD steps (50 ps) and found that only one layer of Si was lithiated. As eight layers of silicon were used in the model, we estimated that at least 400 ps are need for the fully lithaition of $Li_{1.71}Si$ at 300K, which will took several months to finish the simulation with twenty central processing units in the parallel computation. To accelerate the simulation of lithiation process, high temperatures of 1100, 1200, 1300, 1400 and 1500 K were applied during the simulation under the NVT ensemble, in which number of atoms, volume and temperature were kept as constant values. Starting from the initial configuration, the atom positions were relaxed at a given temperature with 15000 MD steps. The time of 15 ps was verified to be sufficient for the full lithiation of Si. A Nosé-Hoover thermostat was applied to the boundary atoms. Mean square displacements (MSD) for the Li and Si atoms as a function of time were calculated to

compute diffusivities of Li and Si atoms at different temperatures, which were then extrapolated to obtain diffusivities of the Li and Si at the room temperature.

The diffusion properties were determined based on the results from the *ab initio* MD calculations. During the lithiation of Si, the positions $r_i(t)$ of all atoms at time t were recorded. The mean square displacements (MSDs) per atom were calculated using the equation (1):

$$MSD = <\left|r_i(t) - r_i(0)\right|^2> = \frac{1}{N}\sum_{i=1}^{N}\left|r_i(t) - r_i(0)\right|^2 \quad (1)$$

where N is the total atomic number and '<···>' denotes the average values over all atoms. The diffusion coefficient (D) at a given temperature was determined using the Einstein relation:

$$D = \lim_{t\to\infty}\frac{MSD}{q_i t} = \lim_{t\to\infty}\frac{1}{q_i t} <\left|r_i(t) - r(0)\right|^2> \quad (2)$$

where q_i is a numerical constant which is dependent on the dimensionality, and q_i = 2, 4, or 6 describes one-, two- or three-dimensional diffusions, respectively. The relationship between the diffusion energy barrier (E_A) and D is based on the Arrhenius equation:[28]

$$D = D_0 \exp(-E_A / k_B T). \quad (3)$$

The values of E_A and D were obtained by fitting the diffusion coefficient with the data obtained using equation (3) at different temperatures.

Acknowledgement:

This work was financially supported by the National Natural Science Foundation of China (11474047). Funding support from Royal academy of Engineering-Research Exchange with China and India is acknowledged.

References:

[1] a) G. L. Soloveichik, *Annual Review of Chemical and Biomolecular Engineering* **2011**, *2*, 503-527; b) J. Liu, *Adv. Funct. Mater.* **2013**, *23*, 924-928.

[2] U. Kasavajjula, C. S. Wang, A. J. Appleby, *J. Power Sources* **2007**, *163*, 1003-1039.

[3] J. R. Dahn, T. Zheng, Y. H. Liu, J. S. Xue, *Science* **1995**, *270*, 590-593.

[4] C. K. Chan, H. L. Peng, G. Liu, K. McIlwrath, X. F. Zhang, R. A. Huggins, Y. Cui, *Nat. Nanotechnol.* **2008**, *3*, 31-35.

[5] J. R. Szczech, S. Jin, *Energy Environ. Sci.* **2011**, *4*, 56-72.

[6] P. R. Abel, A. M. Chockla, Y.-M. Lin, V. C. Holmberg, J. T. Harris, B. A. Korgel, A. Heller, C. B. Mullins, *ACS Nano* **2013**, *7*, 2249-2257.

[7] M. J. Chon, V. A. Sethuraman, A. McCormick, V. Srinivasan, P. R. Guduru, *Phys. Rev. Lett.* **2011**, *107*, 045503.

[8] T. D. Hatchard, J. R. Dahn, *J. Electrochem. Soc.* **2004**, *151*, A838-A842.

[9] H. Li, X. Huang, L. Chen, G. Zhou, Z. Zhang, D. Yu, Y. Jun Mo, N. Pei, *Solid State Ionics* **2000**, *135*, 181-191.

[10] a) C. M. Wang, X. L. Li, Z. G. Wang, W. Xu, J. Liu, F. Gao, L. Kovarik, J. G. Zhang, J. Howe, D. J. Burton, Z. Y. Liu, X. C. Xiao, S. Thevuthasan, D. R. Baer, *Nano Lett.* **2012**, *12*, 1624-1632; b) H. Ghassemi, M. Au, N. Chen, P. A. Heiden, R. S. Yassar, *ACS Nano* **2011**, *5*, 7805-7811; c) X. H. Liu, L. Q. Zhang, L. Zhong, Y. Liu, H. Zheng, J. W. Wang, J. H. Cho, S. A. Dayeh, S. T. Picraux, J. P. Sullivan, S. X. Mao, Z. Z. Ye, J. Y. Huang, *Nano Lett.* **2011**, *11*, 2251-2258.

[11] B. Key, R. Bhattacharyya, M. Morcrette, V. Seznec, J. M. Tarascon, C. P. Grey, *J. Am. Chem. Soc.* **2009**, *131*, 9239-9249.

[12] K. Yoshimura, J. Suzuki, K. Sekine, T. Takamura, *J. Power Sources* **2007**, *174*, 653-657.

[13] A. Kuhn, P. Sreeraj, R. Poettgen, H.-D. Wiemhoefer, M. Wilkening, P. Heitjans, *J. American Chem. Soc.* **2011**, *133*, 11018-11021.

[14] a) N. Ding, J. Xu, Y. X. Yao, G. Wegner, X. Fang, C. H. Chen, I. Lieberwirth, *Solid State Ionics* **2009**, *180*, 222-225; b) R. Ruffo, S. S. Hong, C. K. Chan, R. A. Huggins, Y. Cui, *J. Phys. Chem. C* **2009**, *113*, 11390-11398; c) J. Xie, N. Imanishi, T. Zhang, A. Hirano, Y. Takeda, O. Yamamoto, *Mater. Chem. Phys.* **2010**, *120*, 421-425.

[15] a) W. Wan, Q. Zhang, Y. Cui, E. Wang, *J. Phys.-Condensed Matter* **2010**, *22*; b) Q. Zhang, W. Zhang, W. Wan, Y. Cui, E. Wang, *Nano Letters* **2010**, *10*, 3243-3249; c) Q. Zhang, Y. Cui, E. Wang, *J. Phys. Chem. C* **2011**, *115*, 9376-9381; d) G. A. Tritsaris, K. J. Zhao, O. U. Okeke, E. Kaxiras, *J. Phys. Chem. C* **2012**, *116*, 22212-22216; e) S. C. Jung, Y.-K. Han, *Phys. Chem. Chem. Phys.* **2011**, *13*, 21282-21287; f) O. I. Malyi, T. L. Tan, S. Manzhos, *Appl. Phys. Express* **2013**, *6*; g) Z. Wang, Q. Su, H. Deng, W. He, J. Lin, Y. Q. Fu, *J. Mater. Chem. A* **2014**, *2*, 13976-13982; hS. C. Jung, Y.-K. Han, *Electrochimica Acta* **2012**, *62*, 73-76.

[16] a) P. Johari, Y. Qi, V. B. Shenoy, *Nano Letters* **2011**, *11*, 5494-5500; b) Z. Wang, M. Gu, Y. Zhou, X. Zu, J. G. Connell, J. Xiao, D. Perea, L. J. Lauhon, J. Bang, S. Zhang, C. Wang, F. Gao, *Nano Letters* **2013**, *13*, 4511-4516.

[17] S. C. Jung, D. S. Jung, J. W. Choi, Y.-K. Han, *J. Phys. Chem. Lett.* **2014**, *5*, 1283-1288.

[18] C.-Y. Chou, G. S. Hwang, *Surf. Sci.* **2013**, *612*, 16-23.

[19] a) H. Okamoto, *Bulletin of Alloy Phase Diagrams* **1990**, *11*, 306-312; b) V. B. Shenoy, P. Johari, Y. Qi, *J. Power Sour.* **2010**, *195*, 6825-6830.

[20] V. L. Chevrier, J. W. Zwanziger, J. R. Dahn, *J. Alloy. Compd.* **2010**, *496*, 25-36.

[21] M. Gu, Z. Wang, J. G. Connell, D. E. Perea, L. J. Lauhon, F. Gao, C. Wang, *ACS Nano* **2013**, *7*, 6303-6309.

[22] H. Kim, C.-Y. Chou, J. G. Ekerdt, G. S. Hwang, *J. Phys. Chem. C* **2011**, *115*, 2514-2521.

[23] a) N. Balke, S. Jesse, Y. Kim, L. Adamczyk, A. Tselev, I. N. Ivanov, N. J. Dudney, S. V. Kalinin, *Nano Letters* **2010**, *10*, 3420-3425; b) E. M. Pell, *Phys. Rev.* **1960**, *119*, 1014-1021; c) E. M. Pell, *Phys. Rev.* **1960**, *119*, 1222-1225.

[24] G. Henkelman, B. P. Uberuaga, H. Jonsson, *J. Chem. Phys.* **2000**, *113*, 9901-9904.

[25] G. Kresse, J. Furthmuller, *Comput. Mater. Sci.* **1996**, *6*, 15-50.

[26] J. M. Soler, E. Artacho, J. D. Gale, A. Garcia, J. Junquera, P. Ordejon, D. Sanchez-Portal, *J. Phys.-Condensed Matter* **2002**, *14*, 2745-2779.

[27] N. Troullier, J. L. Martins, *Phys. Rev. B* **1991**, *43*, 1993-2006.

[28] G. J. Janz, U. Kerbs, H. Siegenthaler, *J. Phys. Chem. Ref. Data* **1972**, *1*.

Table 1. Structural parameters for crystalline LiSi, $Li_{12}Si_7$, $Li_{13}Si_4$, $Li_{15}Si_4$ alloys.

			DZ			DZP		
Phase	*x*	Space group	a (Å)	b (Å)	c (Å)	a (Å)	b (Å)	c (Å)
LiSi	1.00	I41/a	9.55	9.55	5.58	9.34	9.34	5.67
$Li_{12}Si_7$	1.71	Pnma	8.44	19.57	14.29	8.51	19.58	14.28
$Li_{13}Si_4$	3.25	Pbam	7.92	14.86	4.39	7.92	15.04	4.43
$Li_{15}Si_4$	3.75	I4-3d	10.55	10.55	10.55	10.65	10.65	10.65

Table 2. Bond length and coordination number (CN) calculated for the first nearest neighbor in crystalline LiSi, $Li_{12}Si_7$, $Li_{13}Si_4$, $Li_{15}Si_4$ alloys.

	Si-Si bond		Li-Li bond		Si-Li bond	
Phase	Length (Å)	CN	Length (Å)	CN	Length (Å)	CN
LiSi	2.45	2	2.76	1	2.67	4
$Li_{12}Si_7$	2.39-2.45	3/2/1	2.5-2.75	3/2/1	2.55-2.65	3
$Li_{13}Si_4$	2.49	1	2.50	1	2.47	2
$Li_{15}Si_4$	--	--	2.61	2	2.61	3

Figure Captions:

Figure 1 Pair correlation functions of Si-Si, Li-Li, and Li-Si for crystalline (a) LiSi, (b) $Li_{12}Si_7$, (c) $Li_{13}Si_4$, and (d) $Li_{15}Si_4$ alloys. Atomistic configurations are shown as insert.

Figure 2 Density of states (DOS) projected on Si and Li atoms in crystalline LiSi, $Li_{12}Si_7$, $Li_{13}Si_4$, $Li_{15}Si_4$ alloys, where the Fermi energy level is set to zero.

Figure 3 Structural snapshots of lithiation of Si to form amorphous $Li_{3.25}Si$ alloy at 1300 K at different simulation times. Green and red balls represent the Si and Li atoms, respectively.

Figure 4 Pair correlation functions of (a) Si-Si, (b) Li-Li, and (c) Li-Si upon lithiation of Si to form amorphous $Li_{3.25}Si$ alloy at 1300 K at different simulation times.

Figure 5 MSD of (a) Li and (b) Si as a function of time upon lithiation of Si to form amorphous $Li_{3.25}Si$ alloy at temperatures 1300 K.

Figure 6 Diffusion coefficients of (a) Li and (b) Si with respect to the inverse of temperature. The value of diffusivity is extrapolated to low temperatures using an exponential fit.

Figure 7 (a) Diffusion barrier and (b) diffusion coefficients show dependence on the composition of Li_xSi alloys at 300 K.

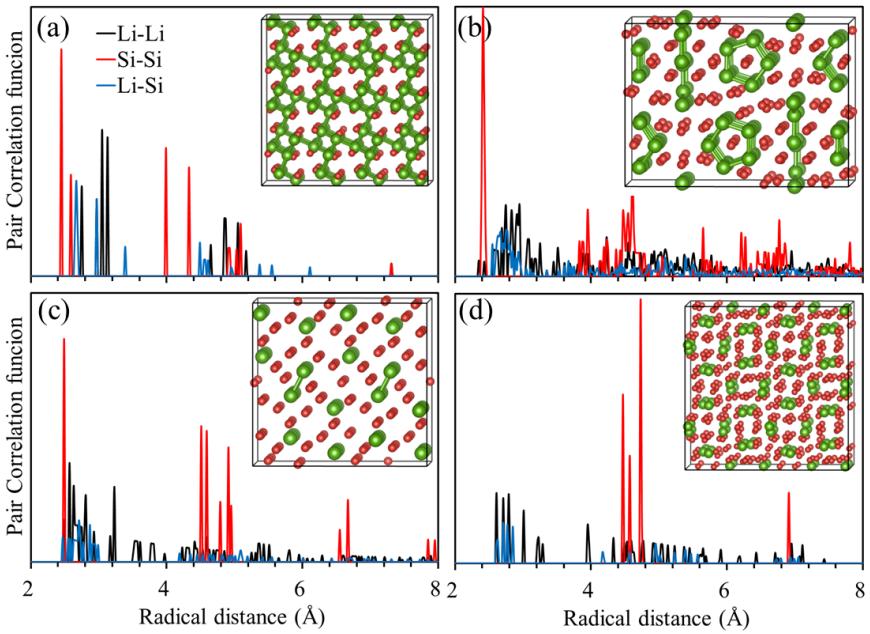

Z.G. Wang et al. Figure 1

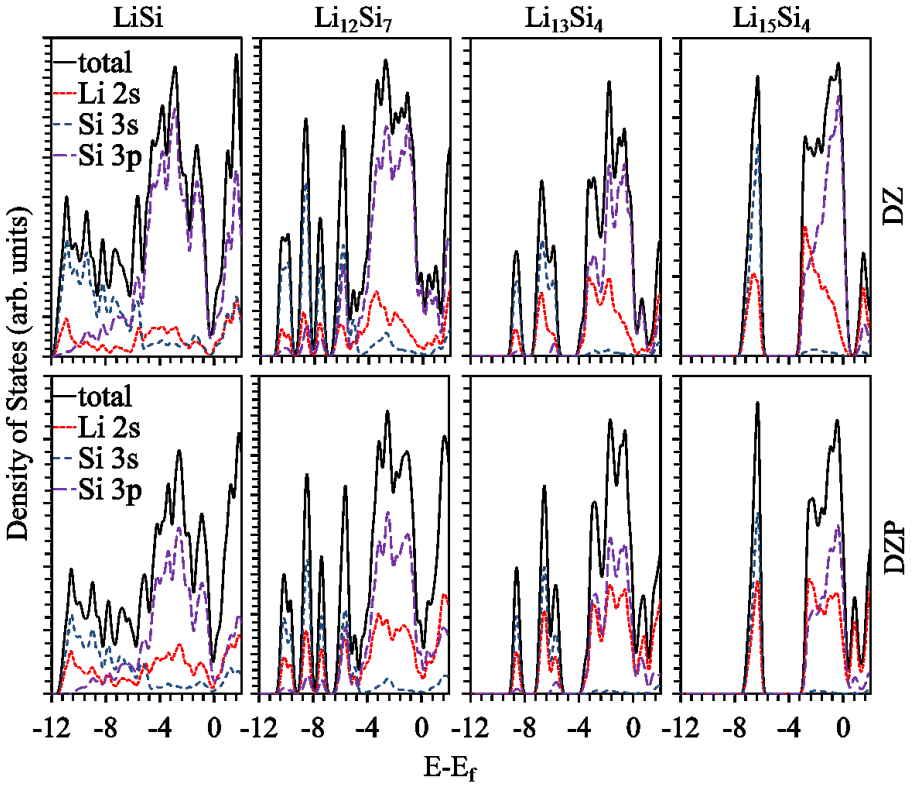

Z.G. Wang et al. Figure 2

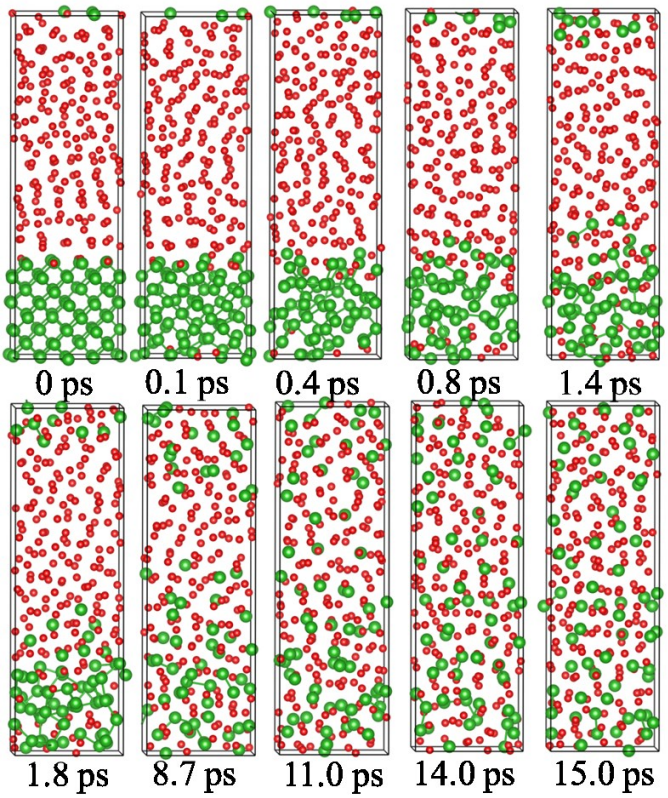

Z.G. Wang et al. Figure 3

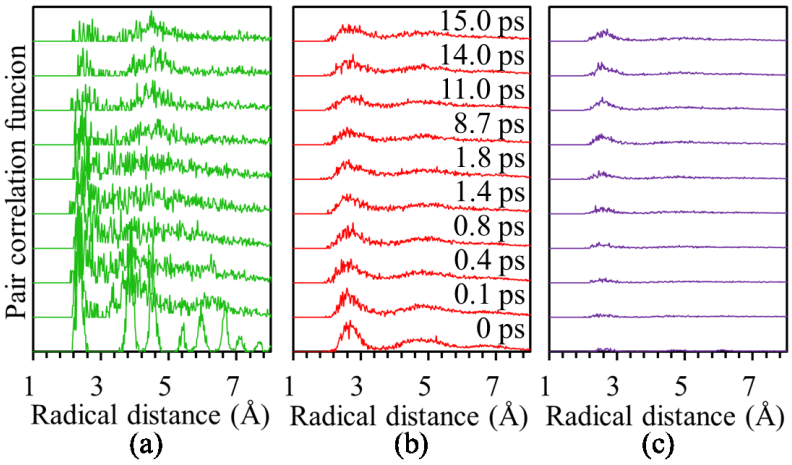

Z.G. Wang et al. Figure 4

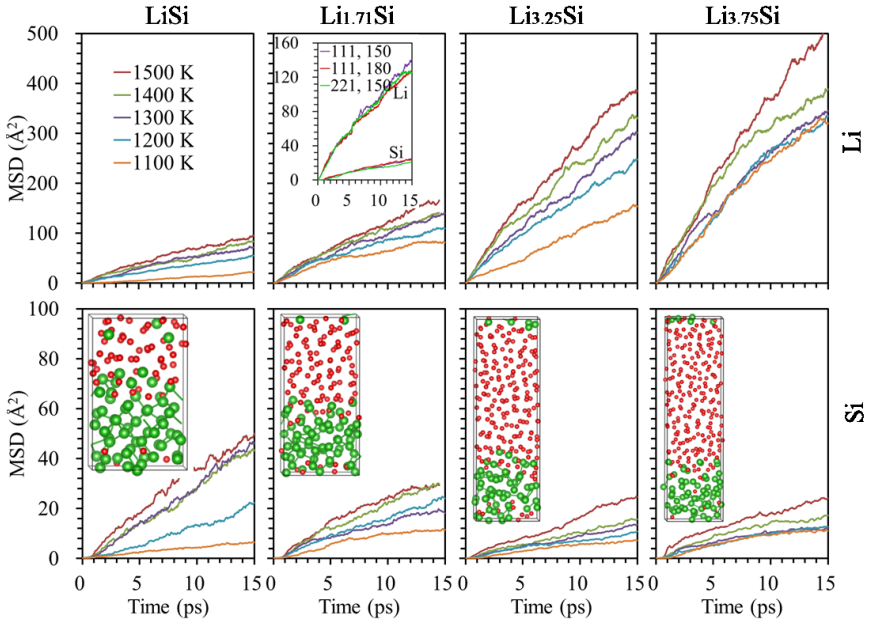

Z.G. Wang et al. Figure 5

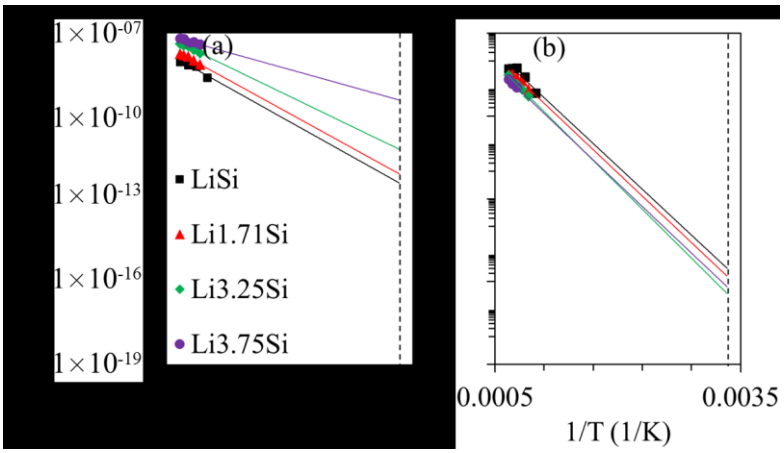

Z.G. Wang et al. Figure 6

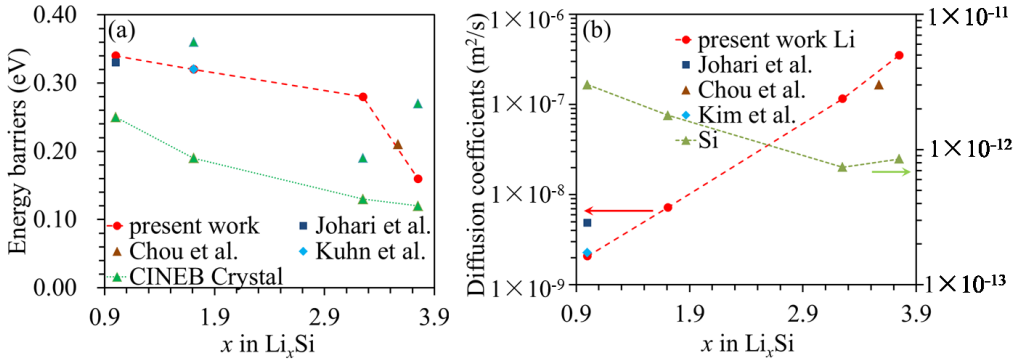

Z.G. Wang et al. Figure 7

Table of content

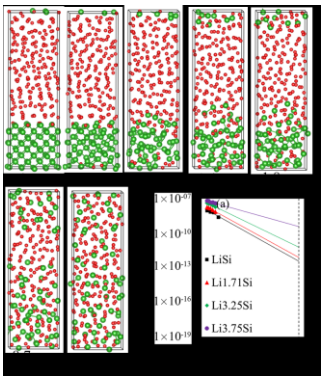
(a)
LiSi
Li1.71Si
Li3.25Si
Li3.75Si